

Simultaneous electrical, UHF, current and optical PD measurements on floating potential under DC stress

Wenger, P.; Abdul Madhar, S.; Beltle, M.

DOI

[10.1109/CEIDP47102.2019.9010548](https://doi.org/10.1109/CEIDP47102.2019.9010548)

Publication date

2019

Document Version

Accepted author manuscript

Published in

2019 IEEE Conference on Electrical Insulation and Dielectric Phenomena, CEIDP 2019 - Proceedings

Citation (APA)

Wenger, P., Abdul Madhar, S., & Beltle, M. (2019). Simultaneous electrical, UHF, current and optical PD measurements on floating potential under DC stress. In *2019 IEEE Conference on Electrical Insulation and Dielectric Phenomena, CEIDP 2019 - Proceedings* (pp. 287-290). Article 9010548 (Annual Report - Conference on Electrical Insulation and Dielectric Phenomena, CEIDP; Vol. 2019-October). <https://doi.org/10.1109/CEIDP47102.2019.9010548>

Important note

To cite this publication, please use the final published version (if applicable). Please check the document version above.

Copyright

Other than for strictly personal use, it is not permitted to download, forward or distribute the text or part of it, without the consent of the author(s) and/or copyright holder(s), unless the work is under an open content license such as Creative Commons.

Takedown policy

Please contact us and provide details if you believe this document breaches copyrights. We will remove access to the work immediately and investigate your claim.

SIMULTANEOUS ELECTRICAL, UHF, CURRENT AND OPTICAL PD MEASUREMENTS ON FLOATING POTENTIAL UNDER DC STRESS

P. Wenger^{1*}, S. Abdul Madhar^{2,3}, M. Beltle¹

¹University of Stuttgart, Stuttgart, 70569 Germany

²Haefely Test AG, Basel 4052, Switzerland

³Delft University of Technology, The Netherlands

*philipp.wenger@ieh.uni-stuttgart.de

Abstract- In this contribution, the partial discharge behavior of two types of floating electrodes under DC stress in air at atmospheric pressure are investigated. Either a hexagonal-shaped nut or a sphere are positioned at a distance of 0.4 mm to the high voltage electrode. The influence of the geometry of the floating electrodes as well as the level and polarity of the applied DC voltage on the partial discharge activity are investigated. Several PD measurement techniques are used simultaneously, namely electrical measurement, ultra-high frequency (UHF) and both high frequency current transformer (HFCT) and shunt measurements. The obtained data is post-processed and visualized with Pulse Sequence Analysis (PSA) diagrams in order to provide characteristic patterns of the investigated defect. In addition, a corona camera detecting the light emissions generated by the discharges provide a further understanding of the defect mechanisms.

I. INTRODUCTION

Partial discharge (PD) measurement is acknowledged being an effective method to diagnose and monitor electrical high voltage equipment under AC stress and has been in practical use for decades. Since the establishment of HVDC operated systems in the power grids, the reliable estimation of the insulation condition for these systems is gaining significance. However, PDs originating from defects under DC voltage are subjected to different physics compared to AC discharge phenomena. Therefore, conventional AC PD measurement methods and evaluation techniques cannot be transferred to DC applications without modifications [1-3].

This paper investigates time synchronized PD measurements using conventional electrical and Ultra High Frequency (UHF) measurement techniques in combination with a corona camera in order to investigate a floating electrode in air. Typical defects causing PD can be voids, surface discharges and metallic conducting components on floating potential [4]. The latter defect may occur if corrosion, mechanical abrasion or an erroneous assembly cause an improper connection of components, joints and electrodes to conductors under high voltage. PD caused by floating potentials represent the scope of this investigation.

The test setup consists of a defined floating electrode, which is located in between a rod-plate electrode arrangement and mechanically supported by an insulating mesh. Different configurations, i.e. dimensions and geometries of the defect are

studied experimentally at both voltage polarities. The magnitude of the applied voltage is increased stepwise from inception ($PDIV$) to $1.3 \cdot V_{inc}$ in order to investigate the discharge behavior at different voltage magnitudes. Evaluation methods tested for PD under DC conditions are pulse magnitude, interval time and repetition rate using Pulse Sequence Analysis (PSA) diagrams.

II. EXPERIMENTAL SETUP AND PROCEDURE

The experimental setup shown in Fig. 1 consists of a DC voltage source, an IEC 60270 conform PD measurement circuit, an UHF measurement system (UHF sensor and fast oscilloscope), HFCT and current shunt measurement system and the test cell with the floating electrode configuration. A rectifier unit supplied by an AC test transformer provides the DC test voltage. The DC voltage can be adjusted continuously in the range of $V_{DC} = \pm 35$ kV.

The specimen shown in Fig. 2 b) consists of a rod-plate electrode configuration with a floating electrode located at a distance of 0.4 mm (hereinafter referred to as small gas gap) from the high voltage electrode. The floating electrode is either a hexagonal nut with a protrusion attached (illustrated in Fig 2 a)) or a sphere with a diameter of $d = 10$ mm. The nut has a length $l = 10$ mm and the radius of the incircle is $r_1 = 4$ mm. The protrusion attached to the nut is directed to the ground electrode and has a diameter $d = 5$ mm and a length $l = 3$ mm. Both electrodes are made of stainless steel. The floating electrode is fixed on an insulating mesh made of low-density polyethylene (LDPE).

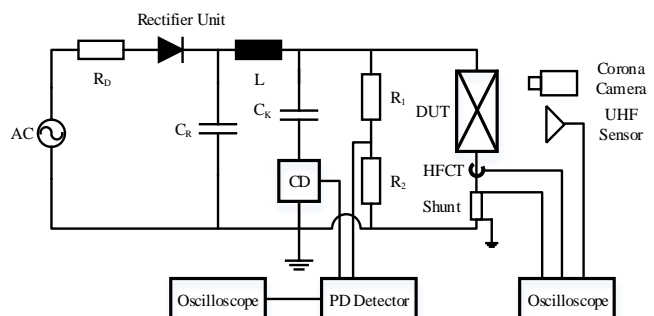


Fig. 1. Schematic of the experimental setup and PD measuring equipment

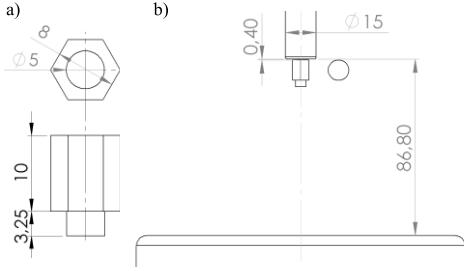


Fig. 2. a) Geometry of floating nut electrode b) Defect configuration with floating nut and sphere electrode at 0.4 mm distance to HV-electrode

Simultaneous measurements of the PD signals in combination with an UV light sensitive camera are performed at constant voltage levels from inception voltage V_{inc} to approximately $1.3 \cdot V_{inc}$. The electrical measurement setup is performed according to the IEC60270 using a coupling capacitor and a measuring impedance in parallel to the DUT [5]. PD signals are recorded using a PD detector (Haefely's Type DDX 9121b), which provides the possibility of pulse streaming through a 'Signal' output-option used for real-time PD measurement. In parallel, an oscilloscope with a 250 MHz bandwidth is used to stream the raw data from the PD Detector and store it on the computer hard-disk for post-processing.

An UHF plate sensor in combination with a fast sampling oscilloscope (40 GSamples/s, 4 GHz bandwidth) is used to record the electromagnetic radiated PD signals. The system is sensitive in the frequency range approx. from 100 to 1800 MHz. The UHF sensor is kept at a constant position and distance to the specimen taking the directivity of the antenna into account.

PD current measurements are carried out in the ground connection of the DUT using either a high frequency current transformer (HFCT) or a current shunt (CS), respectively. The measuring bandwidth of the Fischer F-2000-12 mm HCFT is in the range of 100 to 3000 MHz. While the current shunt has a high frequency cut off (-3 dB) at 20 MHz. Additionally, a corona camera (OFiL Luminar^{HD} Systems), which measures the UV (Ultra Violet) radiation from the discharge site, is used in parallel to provide further insight into the discharge phenomenon. It measures PD's UV emissions in the solar blind range of 250 to 280 nm.

III. SIMULATION OF ELECTRIC FIELD DISTRIBUTION

The ratio of the electric field distribution between the high voltage, ground and floating electrodes depends on the geometry of the floating electrode. The electric field distribution of the electrode configuration with floating potential is calculated using a FEM (Finite Element) simulation tool. For reference, the distribution of the undisturbed electric field without floating electrode is evaluated. The results are illustrated in Fig. 3. The green dash dot lines in the pictograms indicate the axis along which the electric field is evaluated. If the nut electrode is installed the electric field in the small gas gap is more homogeneous distributed along the axis of rotation. However, at the nuts' sharp edges pointing towards the large gas gap the electric field strength is significantly increased and PD is generated.

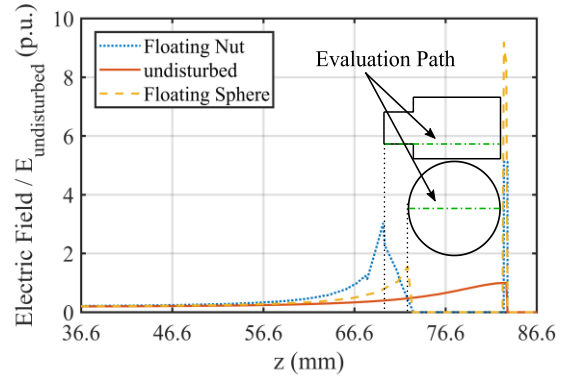


Fig. 3. Distribution of electric field along the axis of rotation in the gas gap without floating electrode, with floating nut and sphere electrode

IV. RESULTS

A. Discharge mechanism of floating electrodes

The PD activity of a floating electrode is mainly depending on the polarity of the applied DC voltage and on the geometry and distance to the high voltage electrode and ground electrode, respectively [6].

Considering the sphere, as a first approximation, the distortion of the electric field due to floating sphere is nearly independent of the diameter, if the sphere is much smaller than the gap length [6]. If an uncharged floating sphere is placed in an electric field (Fig. 4 a), it is charged by a single discharge impulse (Fig. 4 c, Part 1), which bridges the small gas gap between high voltage electrode and floating electrode. Once, the floating sphere is charged, no abrupt discharge occurs, because the floating electrode is charged with the same polarity as the HV electrode reducing the electric field strength over the small gas gap. In the large gas gap between floating electrode and ground electrode, no discharge occurs due to the homogenized distribution of the electric field. However, a very small DC current flows through the large gas gap between floating electrode and ground electrode and discharges the sphere by time (Fig. 4 c, Part 2). With decreasing accumulated charge on the floating potential, the electric field strength in the small gas gap increases. With a time delay in the range of $t_d = 1$ to 2 min PD impulses bridge the small gas gap with amplitudes well over 10s of nC are recorded with the electrical measurement system.

In case of the nut electrode, corona discharges occur at the bottom side, of the floating charged nut electrode (at the protrusion) due to the significantly higher pronounced distortion of the electric field, as shown in Fig. 4 b), Part 2. Recordings taken with a corona camera suggest that the primary discharge occurs between the floating electrode and the high voltage electrode [7]. Under negative polarity, several successive discharges with decreased amplitude occur from the floating electrode directed to the ground electrode. The signal stream in Fig. 5 illustrated the charging and discharging of the floating electrode, which is indicated by the variation of the pulse amplitudes. Under positive polarity just one successive discharge pulse is recorded in most cases forming a pulse stream as illustrated in Fig. 6.

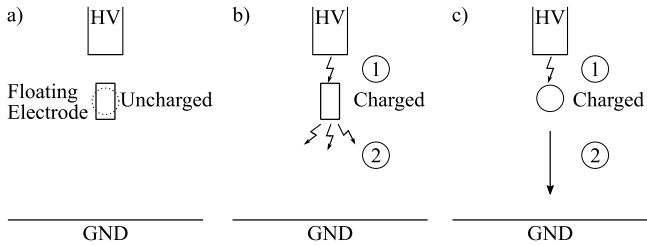


Fig. 4. Discharge characteristic depending on geometry of floating electrodes

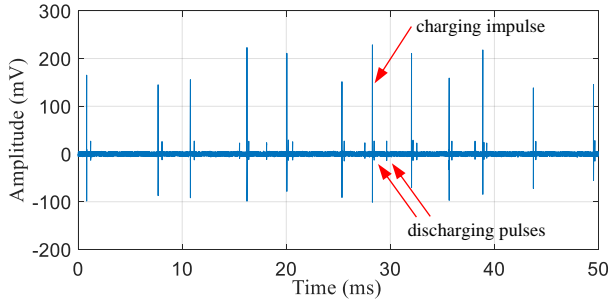


Fig. 5. Sample signal stream of floating nut electrode measured electrically at $V_{DC} = -27.7$ kV

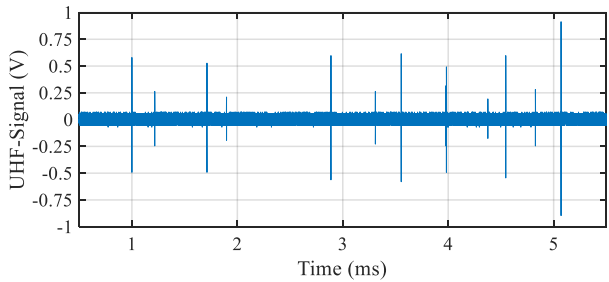


Fig. 6. Sample UHF-PD- signal stream of floating nut electrode measured using UHF sensor at $V_{DC} = +26.8$ kV

B. Negative DC voltage applied to HV electrode with floating nut electrode

PSA diagrams of PD activity of a nut-shaped floating electrode at a constant negative DC voltage are illustrated in Fig. 7. PSA utilizes three successive pulses to deduce differences in discharge magnitude and time between pulses [8]. At inception voltage $V_{inc} = -27$ kV a steady pulse stream with alternating high and low amplitudes is recorded. With increasing applied voltage, the amplitude of PD pulses increases, whereas the time delay between successive pulses decrease. In the PSA diagram of the pulse magnitudes (Fig. 7 a) a significant cluster formation with three sharp edges can be seen as demonstrated previously by other researchers [9]. The difference in the plots developed for UHF and electrical measurement is because some of the discharge impulses occurring from the floating electrode in the large gas gap are not recorded by the UHF sensor. This was confirmed through the current measurements which indicate, that some of the PD pulses have spectral components not exceeding 100 MHz and therefore, cannot be recorded by the UHF and HFCT measuring system.

C. Positive DC voltage applied to HV electrode with floating nut electrode

PSA diagrams of PD activity of a nut-shaped floating electrode with constant positive applied DC voltage to the top electrode are illustrated in Fig. 8. At positive voltage, pulse amplitudes are significantly higher and the pulse repetition rate is reduced. Again, some of the successive discharges forming in the large gas gap cannot be detected with UHF and HFCT measurement techniques due to an input band pass characteristic with lower cutoff frequency at 100 MHz. The electrical measurement detects PD at two different ranges: from 8 to 10 nC and at a small range at approx. 450 pC. The smaller discharge pulses can be localized by visualization using the corona camera as coming from the large gas gap between nut and ground electrode. Pulses with larger magnitude correlate with the charging pulses through the small gas gap. To accommodate these large impulse amplitudes, an external attenuator used at the input terminal of the electrical PD detector. However, the attenuation of the smaller discharge pulses causing them to disappear into the signal's noise floor in some cases. Hence, the plots of the electrical measurement shown in Fig. 7 are slightly distorted from the missing data.

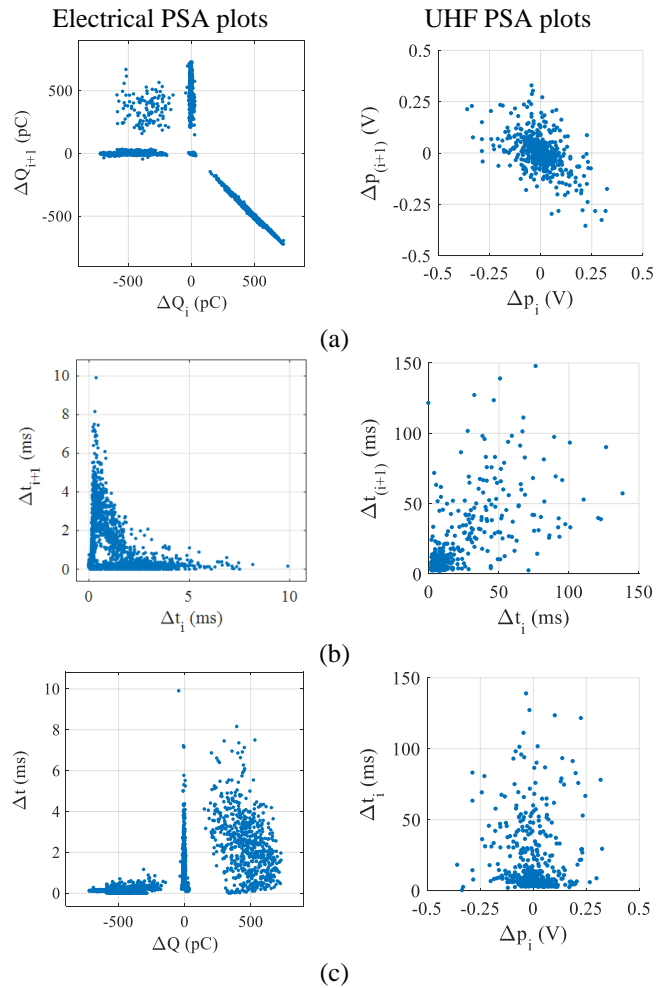


Fig. 7. PSA pattern of floating nut electrode at $V_{DC} = -27.7$ kV; a) correlation of difference in amplitude; b) correlation of difference in time delay; c) correlation of difference in time delay and amplitude

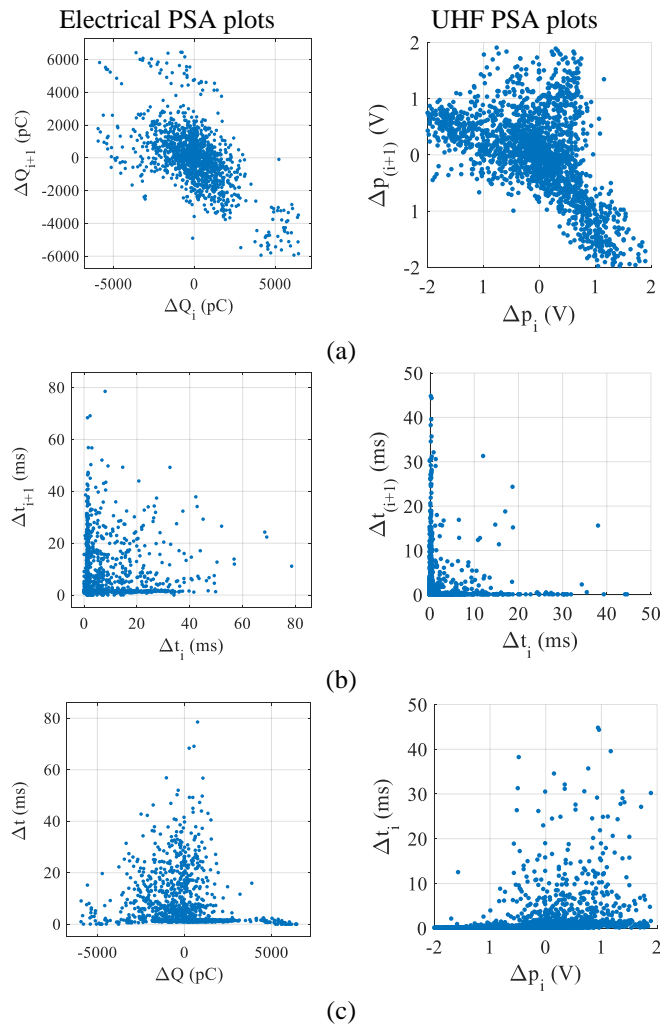


Fig. 8. PSA pattern of floating nut electrode at $V_{DC} = +28.5$ kV; a) correlation of difference in amplitude; b) correlation of difference in time delay; c) correlation of difference in time delay and amplitude

V. CONCLUSION

PD defect mechanisms at floating potentials are dependent on various parameters, such as the geometry and size of the floating potential, its location in the gas gap and level, shape and polarity of the applied voltage. This contribution focuses on the correct detection of PD with a floating electrode in close vicinity to the high voltage electrode at DC excitation. The correct detection is a challenging task, where specific hardware requirements need to be taken into consideration. Under positive DC voltage, PD impulse amplitudes ranging over several nC and can easily exceed the input range of the recording PD detector. Under negative DC voltage, some of the PD pulses have spectral components not exceeding 100 MHz and therefore, cannot be recorded by the UHF and HFCT measuring system. For floating spheres, no corona discharges in the large gas gap occurred and a DC current discharges the sphere over time posing a major safety concern for system operation under DC conditions, as the object remains charged and the condition remains undetected. Correct detection of all PD pulses requires both, an extremely large dynamic range

(vertical resolution) and a suitable lower cut-off frequency of the measurement system to ensure detection of all PD pulses.

The optical evaluation of PD with a corona camera with respect to magnitude of the discharge pulses is not achievable due to the influence of distance and camera perspective to the defect. However, localization of the discharges is possible with high accuracy, which enables the discrimination of the charging (bridging of the small gas gap) and discharging (partially bridging of the large gas gap) impulses of the floating electrode. In combination with electrical and UHF measurement techniques, optical PD detection can provide further understanding of discharge mechanisms of specific defects.

ACKNOWLEDGMENT

This work has partially received funding from the European Union's Horizon 2020 research and innovation program under the Marie Skłodowska-Curie grant agreement No. 676042.

REFERENCES

- [1] H. Saadati, P. Werle, J. M. Seifert, E. Gockenbach, H. Borsi, „Fundamental Difference of Partial Discharge Phenomena under AC and DC Stresses”, IEEE International Conference on High Voltage Engineering and Application, Athens, Greece, September 2018
- [2] U. Lühning, D. Wienold, F. Jenau, “Comparative investigation on pulse shape parameters of partial discharge in air under AC and DC voltage stress”, International Universities Power Engineering Conference, Coimbra, Portugal, September 2016
- [3] R. Piccin, A. R. Mor, P. Morshuis, A. Girodet, J. Snit, “Partial Discharge Analysis of Gas Insulated Systems at High Voltage AC and DC”, IEEE Transactions on Dielectrics and Electrical Insulation, Vol. 22, No. 1, February 2015
- [4] A. J. Reid, M. D. Judd, R. A. Fouracre, B. G. Stewart, D. M. Hepburn, “Simultaneous Measurement of Partial Discharges using IEC60270 and Radio-frequency Techniques”, IEEE Transactions on Dielectrics and Electrical Insulation, Vol. 18, No. 2, April 2011
- [5] High-Voltage Test Techniques – Partial Discharge Measurements, International Standard, IEC 60270:2001 + A1:2016
- [6] M. Kubuki, R. Yoshimoto, K. Tanoue, M. Hara, “Breakdown Characteristics in Air Gaps with Artificial Floating Metals under dc Voltage”, IEEE Transactions on Dielectrics and Electrical Insulation, Vol. 2 No. 1, February 1995
- [7] S. M. El-Makkawy, “Computation of electric stress and corona onset voltage in air gaps with floating particles”, 12th International Middle-East Power System Conference, Aswan, Egypt, March 2008
- [8] M. Hoof and R. Patsch, “Pulse-sequence analysis: a new method for investigating the physics of PD-induced ageing”, IEE Proceedings – Science, Measurement and Technology, Vol. 142, No. 1, pp. 95-101, January 1995
- [9] A. Pirker, U. Schichler, “Partial Discharge Measurement at DC Voltage Evaluation and Characterization by NoDi* Pattern”, IEEE Transactions on Dielectrics and Electrical Insulation, Vol. 25, No. 3, June 2018